International Society for Biofabrication
PURPOSE-LED PUBLISHING™

PAPER • **OPEN ACCESS**

3D bioprinting of mouse pre-osteoblasts and human MSCs using bioinks consisting of gelatin and decellularized bone particles

To cite this article: Aylin Kara Özenler *et al* 2024 *Biofabrication* **16** 025027

Biofabrication

PAPER

3D bioprinting of mouse pre-osteoblasts and human MSCs using bioinks consisting of gelatin and decellularized bone particles

Aylin Kara Özenler[1,2,3,4,*], **Thomas Distler**[2], **Ashwini Rahul Akkineni**[3], **Funda Tihminlioglu**[5], **Michael Gelinsky**[3] and **Aldo R Boccaccini**[2,*]

[1] İzmir Institute of Technology, Department of Bioengineering, İzmir 35433, Turkey
[2] Institute of Biomaterials, Department of Material Science and Engineering, Friedrich-Alexander-University Erlangen-Nuremberg, Erlangen 91058, Germany
[3] Centre for Translational Bone, Joint and Soft Tissue Research, Technische Universität Dresden, Faculty of Medicine and University Hospital, Dresden, 01307, Germany
[4] Department of Orthopedics, University Medical Center Utrecht, Utrecht, 3584 CT, The Netherlands
[5] İzmir Institute of Technology, Department of Chemical Engineering, İzmir 35433, Turkey
* Authors to whom any correspondence should be addressed.

E-mail: a.karaozenler@umcutrecht.nl and aldo.boccaccini@fau.de

Keywords: 3D bioprinting, bone tissue engineering, decellularized bone, gelatin, microbial transglutaminase

Supplementary material for this article is available online

OPEN ACCESS

RECEIVED
30 October 2023

REVISED
29 January 2024

ACCEPTED FOR PUBLICATION
23 February 2024

PUBLISHED
13 March 2024

Abstract

One of the key challenges in biofabrication applications is to obtain bioinks that provide a balance between printability, shape fidelity, cell viability, and tissue maturation. Decellularization methods allow the extraction of natural extracellular matrix, preserving tissue-specific matrix proteins. However, the critical challenge in bone decellularization is to preserve both organic (collagen, proteoglycans) and inorganic components (hydroxyapatite) to maintain the natural composition and functionality of bone. Besides, there is a need to investigate the effects of decellularized bone (DB) particles as a tissue-based additive in bioink formulation to develop functional bioinks. Here we evaluated the effect of incorporating DB particles of different sizes ($\leq$45 and $\leq$100 μm) and concentrations (1%, 5%, 10% (wt %)) into bioink formulations containing gelatin (GEL) and pre-osteoblasts (MC3T3-E1) or human mesenchymal stem cells (hTERT-MSCs). In addition, we propose a minimalistic bioink formulation using GEL, DB particles and cells with an easy preparation process resulting in a high cell viability. The printability properties of the inks were evaluated. Additionally, rheological properties were determined with shear thinning and thixotropy tests. The bioprinted constructs were cultured for 28 days. The viability, proliferation, and osteogenic differentiation capacity of cells were evaluated using biochemical assays and fluorescence microscopy. The incorporation of DB particles enhanced cell proliferation and osteogenic differentiation capacity which might be due to the natural collagen and hydroxyapatite content of DB particles. Alkaline phosphatase activity is increased significantly by using DB particles, notably, without an osteogenic induction of the cells. Moreover, fluorescence images display pronounced cell-material interaction and cell attachment inside the constructs. With these promising results, the present minimalistic bioink formulation is envisioned as a potential candidate for bone tissue engineering as a clinically translatable material with straightforward preparation and high cell activity.

1. Introduction

Biofabrication by extrusion printing methods offers fascinating outcomes for the three-dimensional (3D) production of living tissue structures that contain biological materials, cells and bioactive molecules. Bioinks are cell-based formulations that are suitable to fabricate 3D structures using automated

biofabrication technology and may contain biomaterials and bioactive components [1]. In a bioink formulation, cells are crucial components that are incorporated as single cells, cell pellets or within biomaterials, for instance hydrogels, microcarriers and microparticles. Therefore, the bioink formulation should be cytocompatible to maintain the cell viability and should have suitable material characteristics (e.g. shear thinning, viscosity, easy crosslinkable) to allow the development of suitable 3D layer-by-layer structures.

Maintaining shape fidelity of the 3D-printed constructs while allowing cell proliferation is essential for the production of biological functional constructs in 3D bioprinting applications. Material characteristics in terms of chemical, physical and mechanical properties directly affect the printability, shape fidelity and also cell behavior after bioprinting. Another important challenge is supporting and guiding cell growth toward its natural environment and providing a coherent presence of certain biochemical and biophysical cues to control cell behavior [2]. In bone tissue engineering, collagen-, alginate-, gelatin- and hyaluronic acid-based bioink formulations or combinations of them have been used for successful fabrication of 3D structures [3–6]. In this study, we are particularly interested in gelatin (GEL) which is water soluble, easily processable and contains high concentration of RGD (arginine-glycine-aspartic acid) sequence that allows cell adhesion [7, 8]. GEL is a widely used biomaterial due to its cytocompatibility and enzymatically degradability properties, being suitable for cell proliferation and growth in tissue engineering applications. In addition, it is a thermosensitive biomaterial that undergoes sol-gel transition. Furthermore, it exhibits viscoelastic and shear-thinning behavior which plays an important role in the rheological and physical properties and makes gelatin a proper biomaterial candidate for bioink formulations [9]. As a GEL solution is cooled down from 37 °C to 4 °C, the viscosity increases [10], thus the extrudability of GEL can be optimized by controlling the temperature. Regarding these promising characteristics, it is advantageous to use GEL in a bioink formulation with high cytocompatibility and tunability properties for bioprinting applications. Furthermore, to improve the printability and shape fidelity of pure GEL, it has been used with other natural and synthetic polymers and successful results have been reported for instance methacrylated GEL [11, 12], oxidized alginate (ADA)-GEL [13], GEL-silk [14] and GEL-chitosan [15]. In numerous studies, methacrylated GEL has been used due to the easy cross-linkable property using UV light [16]. In another study, Negrini *et al* demonstrated a GEL biomaterial ink with a different crosslinking approach, N,N′-methylene bisacrylamide (MBA) was used as a crosslinker and included in the GEL solution before 3D printing and the hydrogels were printed on a cooled surface [17]. In addition to those studies, the use of microbial transglutaminase (mTG), a biological enzyme that catalyzes the formation of covalent bonds between the γ-carbonyl group of a glutamine residue and ϵ-amino group of a lysine residue has been proposed, as a crosslinker [18, 19]. A heat treatment step for the preparation of the GEL solution to increase the printability of GEL has been also reported previously [20, 21]. Heat treatment of GEL does not alter the chemical composition of GEL, but reduces its molecular weight via hydrolytic degradation, hence enhancing its rheological printability [20]. Therefore, it could be possible to obtain a minimalistic formulation of ink using heat-treated GEL and mTG as crosslinker.

The incorporation of inorganic materials into polymer matrices is an advanced approach for the development of composite biomaterials or biomaterial ink formulations, especially in bone tissue engineering applications [22, 23]. With high surface area and unique structural shape, inorganic additives can significantly influence the properties of 3D scaffolds with tailored functionalities. In bone tissue engineering, inorganic materials-reinforced bioink formulations have been reported with successful outcomes in many studies using different materials and designs [4, 24–28]. Utilizing both organic and inorganic materials in a composite structure is a suitable approach to mimic the bone tissue extracellular matrix (ECM). On the other hand, decellularization methods enable to obtain biological structures preserving tissue-specific ECM proteins such as collagen and glycosaminoglycan, which can be used in particulate form to enrich bioinks.

In this context, 3D constructs/scaffolds can be produced that better mimic natural tissues using decellularized tissue components. In this study, therefore, we used decellularized bone (DB) particles as an additive in the GEL matrix. The hypothesis is that natural bone ECM proteins and the biomineralization property of bone tissue, preserved by the applied decellularization method [21], will enhance the proliferation and osteogenic differentiation of cells within the bioink formulations. To the best of our knowledge, the development of DB particles incorporated GEL bioinks with pre-osteoblasts and human MSCs, an immortalized human mesenchymal stem cell line [29], and the assessment of the different sizes and concentrations of DB particles in bioink formulations have not been reported yet. Decellularized ECM and collagen-derived GEL are compatible materials that could generate a proper interphase adhesion between the two materials [21]. Regarding these advantages, it could be possible to create a more effective and minimalistic bioink formulation for bone tissue engineering applications.

The aim of this study is to develop such a minimalistic bioink formulation composed of GEL, DB

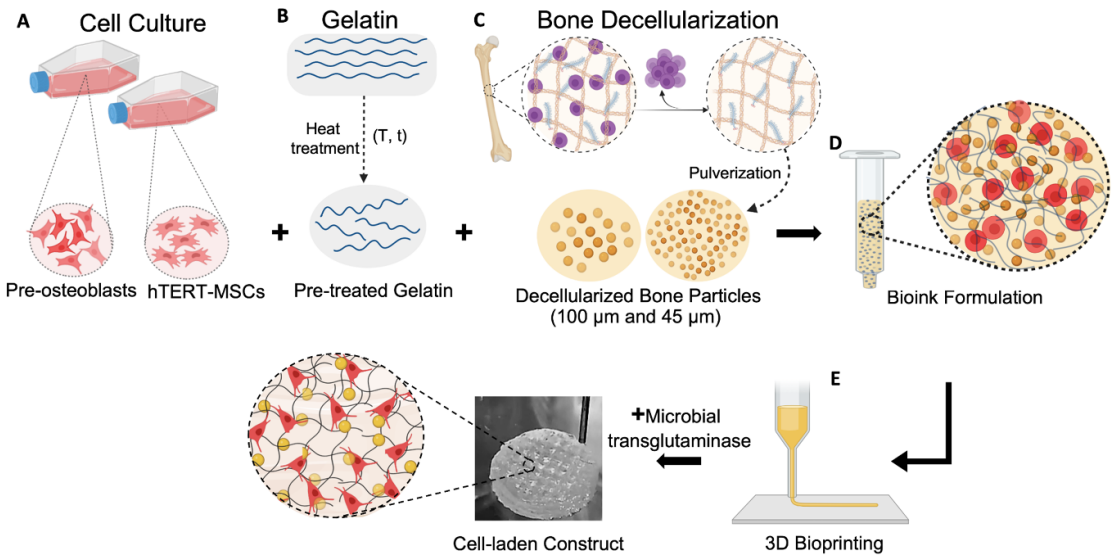

Figure 1. Schematic illustration of the study. (A) MC3T3-E1 pre-osteoblasts and hTERT-MSCs were used for bioink preparation. (B) GEL was prepared, and heat treated to enhance its rheological properties. (C) To prepare tissue-based additives, animal derived bone tissue was decellularized and particles were obtained in different sizes (100 μm and 45 μm) by pulverization. (D) For bioink formulation, cells, pre-treated GEL and DB particles were mixed and (E) cell-laden 3D constructs were fabricated by the 3D bioprinting technique. (Created with BioRender).

particles and cells, and also evaluate the effect of different DB particle sizes and concentrations within the GEL matrix on cell behavior. The schematic illustration of the study is represented in figure 1. In our previous study, we found that DB particles and GEL combinations as biomaterial inks were favorable for MC3T3-E1 pre-osteoblast cells [21]. Here, we tested the GEL/DB composite bioink formulations with mouse pre-osteoblasts (MC3T3-E1) and human telomerase reverse transcriptase-immortalized mesenchymal stem cells (hTERT-MSCs). Different sizes and concentrations of DB particles were incorporated in the GEL matrix to obtain printable formulations and also enhance the cell behavior. As we reported previously, 100 μm particle size mitigates the printability in higher particle concentration [21], therefore, our hypothesis was that reducing the particle size may increase the printability and also cell behavior could increase with higher DB particle concentration. Thus, the effect of different sizes of DB particles was evaluated in two different bioink formulations with different cell types. By crosslinking with mTG, the 3D bioprinted constructs' stability was preserved. All 3D bioprinted cell-laden GEL/DB constructs were evaluated in terms of cytocompatibility, bioactivity and osteogenic differentiation throughout a 28 day culture period.

2. Materials and methods

2.1. Cell culture maintenance

For the preparation of the bioinks and cell culture experiments pre-osteoblast MC3T3-E1 cells (Sigma Aldrich, Catalog number: 99072810, Germany) and human telomerase reverse transcriptase-immortalized mesenchymal stem cells (hTERT-MSCs) were used [29]. MC3T3-E1 cells were subcultured in alpha-modified minimum essential medium (α-MEM, Thermo Fisher, Catalog number: 22571020, Germany), containing 1% (v/v) L-glutamine, 10% (v/v) Fetal Bovine Serum (FBS) and 1% (v/v) penicillin-streptomycin (all supplements: Sigma Aldrich, Germany) in an incubator at 5% CO_2, 95% humidity and 37 °C. hTERT-MSCs were subcultured in Dulbecco's Modified Eagle's Medium (DMEM, Glutamax, Thermo Fisher, Catalog number: 61965059, Germany) with high glucose supplemented with 10% (v/v) FBS and 1% (v/v) penicillin-streptomycin. The cell culture medium was refreshed twice a week.

2.2. Preparation of bioinks

Bone tissues were obtained from New Zealand White Rabbit's femur (weight, 2.5–3.0 kg; female) in accordance with the protocol accepted by Dokuz Eylul University Experimental Animals Ethical Council (İzmir, Turkey, protocol no: 44/2019). Also, bovine bones were obtained from a slaughterhouse in Izmir to obtain a high amount of particles. Bone tissues were decellularized by a combination of physical, chemical, and enzymatic methods reported in our previous study [21]. Decellularized bone (DB) pieces were pulverized using a laboratory mixer and filtered with 45 μm and 100 μm mesh diameters to prepare different sizes of particles. DB particles were sterilized using gamma radiation (25 kGy). 15% (w/v) gelatin (GEL, from porcine skin, gel strength 300, Type A, Sigma, Catalog number: G2500) was dissolved in ultrapure water at 80 °C for 3 h and filtered using

a syringe filter with 0.02 μm for sterilization. Rabbit DB particles were used to prepared GEL/1%DB (w/v, 100 μm size) inks, and bovine DB particles were used for GEL/5%DB (w/v, 45 μm and 100 μm size) and GEL/10%DB (w/v, 45 μm size) inks (SI, table 1). DB particles were prepared by dispersing in ultrapure water under stirring at 37 °C. Then, a final concentration of 7.5% (w/v) GEL was prepared by mixing with DB particles at room temperature for 15 min using a magnetic stirrer. For bioink formulation, cell pellets (5×10^6 cells ml^{-1}) were prepared by using a centrifuge at 1250 rpm then cell pellets and GEL/DB composite inks were mixed. Pure GEL served as a control group. Besides, GEL and GEL/1%DB (w/v) bioinks prepared with MC3T3-E1 cells were cast into 12 well-plates for the 2D control group. For bioprinting of MC3T3-E1 cells, the GEL/1% DB (particles in 100 μm size (w/v)) formulation was used. As we proved the initial cytotoxicity of GEL/DB formulation with MC3T3-E1 cells and high cell-particle interaction in our previous study [20], hTERT-MSCs as a more biological relevant cell type were bioprinted using GEL containing 5% DB (100 μm size, (w/v)), 5% DB (45 μm size, (w/v)) and 10% DB (45 μm size, (w/v)) bioink formulations, and the effect of different DB particle sizes and concentrations on different cell sources was evaluated. Thus, different bioink formulations were investigated using murine MC3T3-E1 cells and human MSCs within GEL-based bioinks contains rabbit and bovine DB particles.

2.3. Rheological characteristics

The rheological characteristics of the prepared biomaterial inks were assessed by shear thinning and shear recovery tests using a rheometer equipped with a plate–plate geometry (Rheotest RN 4, Germany). Shear thinning tests were performed at room temperature (25 °C) with a constant increase in shear rates from 0 to 100 s^{-1} (increment of 0.1 s^{-1} per second). To evaluate the structural recovery of the material inks, thixotropy tests were carried out, which comprised of three phases: a transient phase (5 s^{-1} shear rate subjected for 120 s), a loading phase (500 s^{-1} shear rate subjected for 60 s), and a recovery phase (5 s^{-1} shear rate subjected for 120 s). The entire thixotropy test was performed at room temperature.

2.4. Printability assessments

The printability accuracy of the prepared biomaterial inks was evaluated semi-quantitatively prior to bioprinting. GEL and GEL/DB biomaterial inks were printed using the same parameters of bioprinting. Light microscopy (M205 C Leica, Germany) images were recorded after printing. The printability of the biomaterial inks was assessed according to the printability (Pr) factor, uniformity (U) factor, pore size and strand diameter of the printed hydrogels. The printability factor based on the circularity (C) of the pore was quantified as the ratio of the pore perimeter (L) to the pore area (A) using the equation below [30]:

$$\mathrm{Pr} = \frac{\Pi}{4} \times \frac{1}{\mathrm{C}} = \frac{\mathrm{L}^2}{16\mathrm{A}}. \quad (1)$$

The uniformity of printed strands was quantified by the U factor which equals to the measured horizontal length of a printed hydrogel strand (L) divided by the theoretical horizontal length of a parallel printed strut (L_t) [31]:

$$\mathrm{C} = \frac{\mathrm{L}}{\mathrm{L_t}}. \quad (2)$$

2.5. 3D bioprinting

3D cylindrical-shaped cell-laden hydrogels were fabricated by using a 3D extrusion bioprinter (Bioscaffolder 3.1, Gesim GmbH Germany). Before bioprinting, the temperature of the cartridge holder was set to room temperature (25 °C) to stabilize the material viscosity. GEL and GEL/DB bioinks were transferred into the cartridge and extruded through the 410 μm nozzles with a tip velocity of 10 mm s^{-1} and extrusion pressure 150–180 kPa. All samples were bioprinted in 5 layers with 0.3 mm layer height and 10 mm diameter. 3D-bioprinted constructs were crosslinked using 10% w/v mTG (85–135 U mg^{-1}, ACTIVA WM, Ajinomoto) for 15 min at room temperature and washed with Hank's balanced salt solutions (HBSS, Gibco Life Technologies, Germany). Then culture medium (described above) was added. 3D-bioprinted constructs were cultured for 28 d in an incubator at 37 °C.

2.6. Cytotoxicity

The potential cytotoxicity of the materials was assessed by the lactate dehydrogenase (LDH) kit (CytoTox Toxicity kit, Promega, Catalog number: G1780). To quantify extracellular LDH release, the cell culture medium was collected from samples and mixed with a substrate solution. Following the incubation of the samples at RT for 30 min in the dark, the absorbance at 490 nm was measured using a spectrophotometer (Infinite M200 PRO, Tecan, Switzerland).

2.7. Cell viability assay

The water-soluble tetrazolium salt (WST-8) assay was performed to determine the viability of cells inside the bioprinted constructs by conversion of the water-soluble tetrazolium salt through cellular metabolism into the insoluble formazan. Samples were cultured for 28 d and at each time point (days 1, 7, 14, 21, 28), the medium was removed, and cell-laden constructs were incubated with WST-8 solution (Cell Counting Kit-8, Sigma Aldrich, Germany) for 3 h according to the manufacturer's instructions. After incubation,

100 μl aliquots were transferred into a 96-well plate and the absorbance at 450 nm was recorded using a plate reader (Infinite M200 PRO, Tecan, Switzerland).

2.8. Live/Dead staining

The cell viability was determined by Live/Dead staining during the cell culture period. Initially, 3D-bioprinted constructs were washed with HBSS and incubated in HBSS containing 0.6 μl ml^{-1} Calcein AM and 1.2 μl ml^{-1} ethidium homodimer-1 (InvitrogenTM, Life Technologies, Catalog number: L3224) for 30 min at 37 °C, 5% CO_2 in a humidified atmosphere. To stain the cell nuclei, 1 μl ml^{-1} DAPI (4′,6-diamidino-2-phenylindole, Invitrogen, USA) was used. After 30 min incubation, samples were washed with HBSS and examined by fluorescence microscope (AxioScope A1, Carl Zeiss, Germany).

2.9. PicoGreen assay

The cell proliferation inside the 3D-bioprinted GEL/DB constructs was determined based on the quantifying of the double-strand DNA (dsDNA) by Quant-iT PicoGreen ds-DNA Assay-Kit (Invitrogen, ThermoFisher, Catalog number: P7589). Cell-laden constructs were incubated for the 28 d culture period. The samples were transferred into Precellys tubes containing ceramic beads (Peqlab, Erlangen, Germany). After adding a cell lysis buffer (1% TritonX-100 in PBS), tubes were shaken for 30 s at 5000 rpm three times using a cell homogenizer (Precellys 24 system, Peqlab). Cell lysates were transferred into a 96-well plate and mixed with a working solution according to the manufacturer's protocol. After 5 min incubation at room temperature, protected from light, the relative fluorescence was recorded at 485 and 535 nm using a spectrofluorometer (Infinite M200 PRO, Tecan, Switzerland).

2.10. Osteogenic activity

The osteogenic differentiation capacity of cells in 3D bioprinted constructs was determined by alkaline phosphatase (ALP) activity, using colorimetric assay to quantify the reaction of colorless p-nitrophenyl phosphate (pNpp) to yellow p-nitrophenolate (pNp) mediated by ALP. 3D-bioprinted constructs were cultured in DMEM with 10% FCS and penicillin-streptomycin for 3 d. Afterward cultured in osteogenic induction media (DMEM with 10% FCS, 1% penicillin-streptomycin, 10 mM β-glycerophosphate, 10^{-7} M dexamethasone, and 0.05 mM ascorbic acid 2-phosphate, denoted as +OS) or basal media (DMEM with 10% FCS and 1% penicillin-streptomycin) were applied for 28 d. On days 7, 14, 21 and 28, cell-laden constructs were lysed in 1% TritonX-100 using Precellys system as described in '*2.9 PicoGreen Assay*'. Cell lysates were incubated in substrate solution for 30 min at 37 °C as reported previously [32]. 1 M NaOH was used to stop enzymatic reaction then the absorbance was recorded at 405 nm using a microplate reader (Infinite M200 PRO, Tecan, Switzerland). The total ALP activity was calculated in relation to cell number obtained from PicoGreen assay measurements.

2.11. Assessment of cell morphology and attachment

3D-bioprinted constructs were examined with fluorescence microscopy and confocal microscopy to assess cell morphology and attachment. Cell-laden constructs were fixed using 4% paraformaldehyde (v/v) in HBSS for 30 min at room temperature protected from light, then washed with HBSS. For permeabilization, samples were immersed in 0.1% Triton X-100 for 5 min and blocked using 1% bovine serum albumin (BSA; Albumin Fraction V, Roth, Germany) for 1 h. Then, samples were stained with 3 μl ml^{-1} phalloidin-i Fluor 488 (Abcam, USA) and 1 μl ml^{-1} DAPI (Gibco, Germany) for 1 h. Following the washing with HBSS, cells inside the GEL/DB constructs were observed by fluorescence microscopy (Zeiss Observer Z1) and confocal microscopy (Leica TCS SP5).

2.12. Statistical analysis

Experimental data are presented as mean ± standard deviation (SD). Statistical analysis was performed using a one-way analysis of variance (ANOVA) with Tukey's multiple comparison test (GraphPad Prism 9.0). All p-values less than 0.05 were considered to be significant ($p < 0.05$) which were defined as $^{*}p < 0.05$, $^{**}p < 0.01$, $^{***}p < 0.001$, $^{****}p < 0.0001$.

3. Results and discussions

3.1. Rheological characteristics

Rheological characteristics of GEL and DB incorporated GEL biomaterial inks were evaluated to mimic the ink flow condition relevant for the printing process. Shear thinning tests were performed for each group measuring the viscosity by increasing the shear rate from 0 to 100 s^{-1}. Figure 2 A displays the viscosity decreased while the shear rate increased for all biomaterial inks which indicates that all materials exhibited suitable shear-thinning behavior for extrusion-based 3D printing. The viscosity of GEL at a shear rate of 10 s^{-1} was determined as 74 Pa.s with statistically significant differences compared to the DB particles incorporated groups (figure 2(B)). Also, the addition of DB particles in different sizes and concentrations influenced the viscosity. The viscosity of GEL/1 DB (100 μm), GEL/5 DB (100 μm), GEL/5 DB (45 μm) and GEL/10%DB (45 μm) was determined as 91.70, 111.61, 123.84 and 170.67 Pa.s, respectively, and statistically significant differences were found (figure 2(B)). DB particles in 45 μm size increased the viscosity compared to 100 μm DB particles incorporated inks with statistical differences indicating that

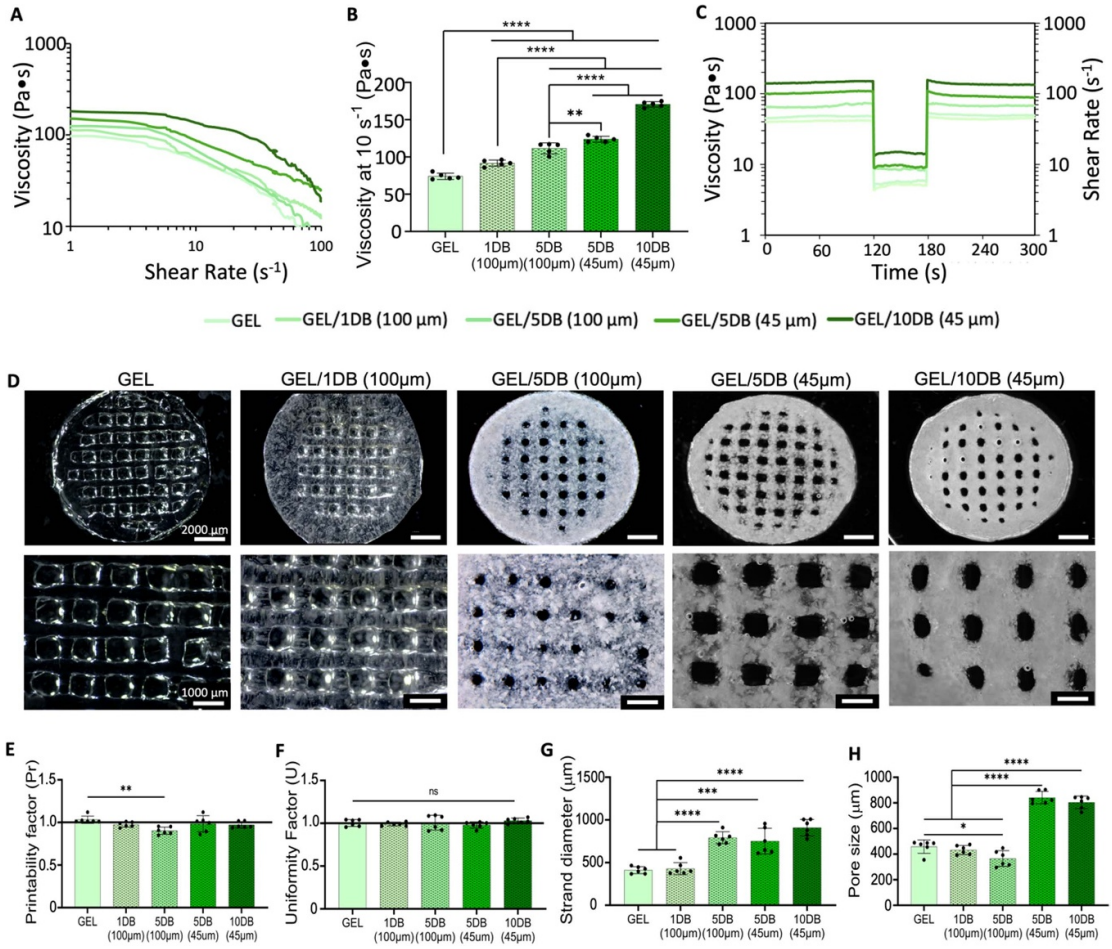

Figure 2. Rheological characteristics of inks and 3D printed hydrogels with the assessment of printability. (A) Representative curves of viscosity obtained from shear thinning tests. (B) The viscosity of the inks at a shear rate of 10 s^{-1}. (C) Thixotropy test results showing transient, loading and recovery phases. All tests were performed using five replicate samples and data are represented as mean ± SD. (D) Light microscopy images of 3D-printed GEL and GEL/DB composite hydrogels. Scale bars: 2000 μm (top), 1000 μm (bottom). Printability assessments of hydrogels ($n = 6$) based on the measurement of (E) Pr and (F) U factors, (G) strand diameter and (H) pore size. Data are shown as mean ± SD. $^{*}p < 0.05$, $^{**}p < 0.01$, $^{***}p < 0.001$ and $^{****}p < 0.0001$ indicate statistically significant differences compared to 3D printed structures by one-way ANOVA tests.

smaller particle sizes enhance the rheological characteristics. Notably, 10% DB incorporated inks exhibited higher viscosity, as shown in figure 2(B). This might be due to the interactions between particles inside the inks. Shear thinning behavior occurs when the interaction between solid particles in composite ink formulations is disrupted by shear forces. The higher viscosity of the ink at rest, determined by the re-organization of interactions between suspended particles, provides shape stability [33, 34]. Thus, higher concentrations of DB particles with smaller sizes allowed dense interactions, between suspended particles which lead to higher viscosity. Moreover, in our previous study, we reported that higher DB particle concentration (>5%) decreased the printability capacity, on the other hand high concentration of DB particles supported cell growth [21]. Here, we showed that the smaller sizes of DB particles in higher concentrations enhance the rheological characteristics which was one of the hypotheses of this study.

The shear recovery capacity of the biomaterial inks was evaluated with thixotropy tests. Three-interval thixotropy test results demonstrate that GEL and DB incorporated GEL inks exhibit shear recoverable properties, indicating that the inks can maintain their structure after 3D printing (figure 2(C)). In the transient phase as the first interval, all materials exhibited a constant viscosity while maintaining their stability at a constant shear rate (5 s^{-1}). After applying a high (500 s^{-1}) shear rate during the loading phase, the viscosity decreased, simulating the printing process where the ink comes out of the nozzle. In the recovery phase, full recovery was achieved for all inks indicating thixotropic behavior when applied 5 s^{-1} shear rate as in the initial first interval (figure 2(C)). The concentration and particle size of DB did not influence the self-recovery capacity of the inks. According to rheological test results, heat-treated pure GEL inks have a suitable viscosity and well-shaped recovery

properties, this is the case also for DB incorporated composite inks. As reported previously, heat treatment allows to enhance shear thinning behavior of GEL by hydrolysis of the chemical bonds without any altered chemical structures [20]. This treatment might be a major factor as pure GEL exhibited appropriate rheological properties for 3D printing. This process might be the main factor that enhances viscosity to make the GEL printable and leads to suitable rheological properties of both GEL inks as well as DB incorporated inks. According to the rheological test results, pure GEL and DB particles incorporated-GEL inks exhibit a shear-thinning behavior and self-recoverability, which indicates that all prepared inks are printable and are suitable for extrusion-based 3D printing.

3.2. 3D printed GEL/DB scaffolds

The printability was assessed on GEL and GEL/DB inks. Light microscopy images display 3D-printed GEL and GEL/DB hydrogels in different sizes and concentrations after crosslinking with transglutaminase (figure 2(D)). Hydrogels were fabricated in a cylindrical shape with alternating 0°/90° strut patterns, resulting in square macropores between the strands. 3D printed GEL and GEL/DB hydrogels exhibited well-printed structures with square pore geometry (figure 2(D)). It was easy to print all inks, notably smaller size of the DB particles (45 μm) in higher concentration was facilitated the printability, which could be the result of the interaction between suspended smaller DB particles homogeneously distributed in the GEL matrix. GEL/DB hydrogels exhibited increasing turbidity in higher particle concentrations despite the transparency of pure GEL hydrogels (figure 2(D)). The printability factor (Pr) was calculated by equation (1) for all groups. $Pr < 1$ indicates under-gelation of the ink and rounded pore corners, $Pr = 1$ indicates proper gelation with ideal square pore geometry, whereas $Pr > 1$ corresponds to over-gelation of the ink [30]. Pr factor was close to 1 in all groups. 5% DB incorporated GEL groups exhibited rounded pore geometry with a lower Pr factor ($Pr = 0.9 \pm 0.04$) and statistical difference was detected compared to the pure GEL hydrogels (figure 2(E)). 3D printed hydrogels demonstrate proper strand morphology when the Pr factor is in the range of 0.9 and 1.1, as reported previously [30]. As a result, 5% DB particles in 100 μm size mitigated the 3D printability while a 5% DB particle concentration in 45 μm size indicated optimal printability. Additionally, 5% DB particles in 45 μm size showed a 0.9 Pr factor with adequate printability capacity and shape fidelity. Reducing particle size to 45 μm improves the printability in the 5% DB group with no statistically differences compared to the pure GEL group. The Pr factor of 10% DB group (45 μm size) was close to 1 and showed a well-shaped 3D structure. However, 10% DB particles of 100 μm size were not able to be incorporated into the GEL matrix homogenously due to precipitation of the particles and it was not possible to print due to the needle clogging. Therefore, the GEL/10% DB group was not included in this study. The quantification of the U factor demonstrated that all printed hydrogels have similar uniformity, and no statistical differences were detected (figure 2(F)). The addition of different concentrations and sizes of DB particles influences the strand diameter and pore size of the printed hydrogels. In concentrations of 1% and 5% DB particles strand size increased with a statistically significant difference while no statistical differences were found between pure GEL and 1% DB incorporated GEL groups (figure 2(G)). In the 5% concentration, the smaller size of particles (45 μm) decreased the strand diameter, higher concentration of particles (10%) slightly increased the strand diameter which could be caused by the surface area of the DB particles; however, no statistical differences were found (figure 2(G)). The strand diameter of pure GEL and 1% DB incorporated GEL showed similar pore sizes, 400 $\pm$ 19 μm, and 431 $\pm$ 30 μm, respectively. The smaller particle sizes exhibited larger pores in both 5% and 10% DB incorporated groups and statistical differences were found compared to the other groups (figure 2(H)). In accordance with the literature, pore size of $\sim$400 μm is suitable for bone tissue engineering [32]. Lee *et al* showed the addition of nanoparticles into alginate-based inks enhanced the uniformity of the strands with high printing fidelity which resulted in high printability capacity [35]. Moreover, they incorporated cationic silica particles into an anionic alginate-gellan gum mixture and demonstrated the improvement in printability and shape fidelity due to the electrostatic interaction between inorganic particles and the biopolymer matrix [36]. In our study, we included DB particles containing collagen fibers in the collagen-derived GEL matrix, as a result of which secondary interactions may occur due to the identical chemical composition of both materials. With this interaction, printability capacity could be enhanced, and shape fidelity could be maintained. In another study, Bednarzig *et al* investigated the effect of the different geometry of hydroxyapatite and bioactive glass particles on the printability properties of alginate-based biomaterial inks and showed that round glass particles containing inks affected the rheological properties, which led to a limited printability capacity compared to angular particles [22]. In accordance with these studies, non-homogeneous shape of DB particles could lead to easier printing of GEL/5 DB and GEL/10 DB. Moreover, sufficient rheological properties obtained after heat treatment of GEL (figures 2(A)–(C)) could lead to better extrudability resulting in well-shaped 3D structures.

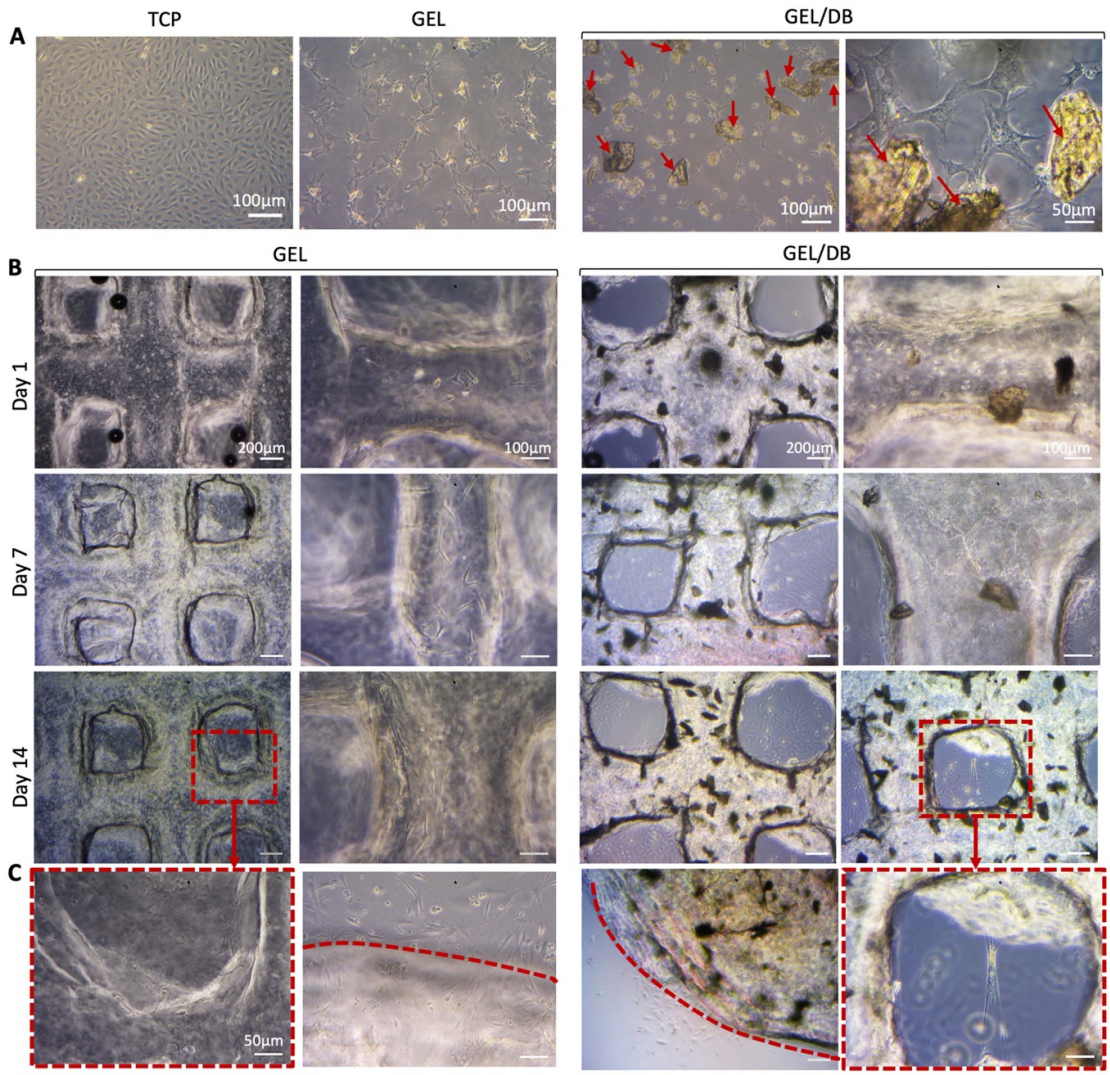

Figure 3. Light microscopy images of cell-laden 2D cast and 3D-bioprinted constructs. (A) Phase contrast light microscopy images of MC3T3-E1 cells seeded on 2D on TCP and in 3D, inside a droplet of GEL and 1% DB particles, on the well plate after 7 d of incubation. Red arrows indicate the DB particles. Scale bars: 100 μm, 50 μm (right magnified image). (B) MC3T3-E1 cells inside the 3D-bioprinted GEL and GEL/1%DB constructs after days 1, 7 and 14. Scale bars: 200 μm (first column), 100 μm (second column). (C) Magnified images of cells showing cell growth in 3D-bioprinted constructs on day 14. Red dotted lines show the edges of the printed constructs, indicating that cells migrated out of the scaffolds at day 14. Scale bars: 50 μm.

3.3. 3D bioprinted MC3T3-E1 pre-osteoblasts-laden GEL/DB constructs

3.3.1. Cell viability

MC3T3-E1 pre-osteoblast cells-laden 1% GEL/DB constructs were fabricated successfully and cell distribution and localization inside the constructs observed by light microscope during the cell culture period. Figure 3 displays light microscopy images of cells inside the GEL and GEL/DB constructs, and TCP (tissue culture polystyrene) control as well. Before bioprinting, 2D cast GEL and GEL/DB hydrogels containing MC3T3-E1 were prepared to observe the cells in hydrogels. As the GEL hydrogels are completely transparent, it was not easy to distinguish the edges of the hydrogels. As seen in figure 3(A), cells are visible in both GEL and GEL/DB hydrogels and attached and elongated cells were observed after 7 d (figure 3(A)). Besides, it was observed that cells attached to the DB particles within the GEL/DB hydrogels (figure 3(A)) [21]. In 3D bioprinted samples, MC3T3-E1 cells were distributed inside both GEL and GEL/1% DB constructs, and they proliferated during the cell culture period (figure 3(B)). Moreover, after 14 d, cells migrated on the construct surface and completely covered the 3D-bioprinted constructs as seen in magnified images in figure 3(C). GEL hydrogels degrade after 14 d and started to lose weight in cell culture medium as reported in a previous [21]. Due to the starting of the degradation of GEL cells could find space inside the 3D-printed constructs and could migrate inside the construct. During the culture period, with the degradation of the constructs in which cells proliferated, the cells migrated outside of the constructs and were observed in the cell culture plate as seen in the magnified images (figure 3(C)). Furthermore, the specific RGD sequence of GEL [37]

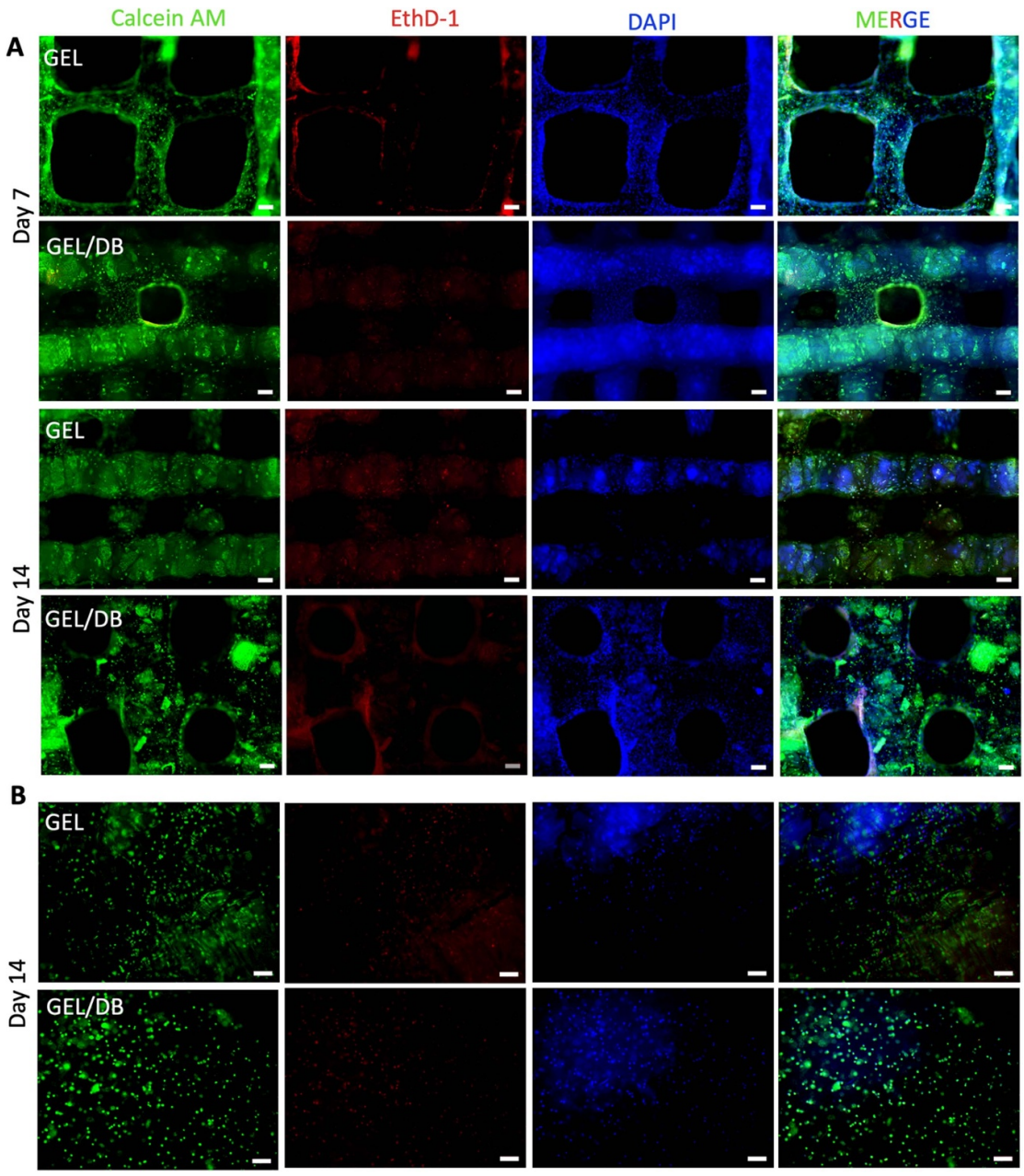

Figure 4. Live/Dead staining results of MC3T3-E1 cells inside the (A) 3D bioprinted constructs on days 7 and 14. (B) Live/Dead staining of MC3T3-E1 cells in 2D cast hydrogels. Calcein AM; live cells (green), EthD-1; dead cells (red), DAPI; cell nuclei (blue). Scale bars: 100 μm.

allowed cells to adhere and proliferate throughout the culture period, demonstrating the cytocompatibility of the GEL and GEL/DB bioink formulation.

In 3D biofabricated constructs, maintaining the cell viability and shape-fidelity or stability of the 3D printed constructs is an important key factor. Therefore, the viability of MC3T3-E1 cells inside the 3D bioprinted constructs was observed after Live/Dead staining during the culture period. Fluorescence microscopy images show live cells (green), dead cells (red) and cell nuclei (blue) (figure 4). DB particles were also visible as blue/green due to their autofluorescence. The images demonstrate that MC3T3-E1 cells attached and maintained their viability inside both GEL and GEL/DB constructs on day 7 (figure 4(A) and SI figure 3). After 14 d, cells attached and spread more inside the constructs and only a few dead cells were observed (figure 4(A)). After 14 d of culture, DAPI staining indicates dense cell nuclei. Also, MC3T3-E1 cells inside 2D cell-laden GEL and GEL/DB hydrogels maintained their viability on day 14 (figure 4(B)). Live/Dead staining results confirmed that the GEL and GEL/DB ink formulations were cytocompatible and did not impair MC3T3-E1 cell viability.

The possible cytotoxic effect of the inks was assessed with LDH cytotoxicity assay during 28 d of

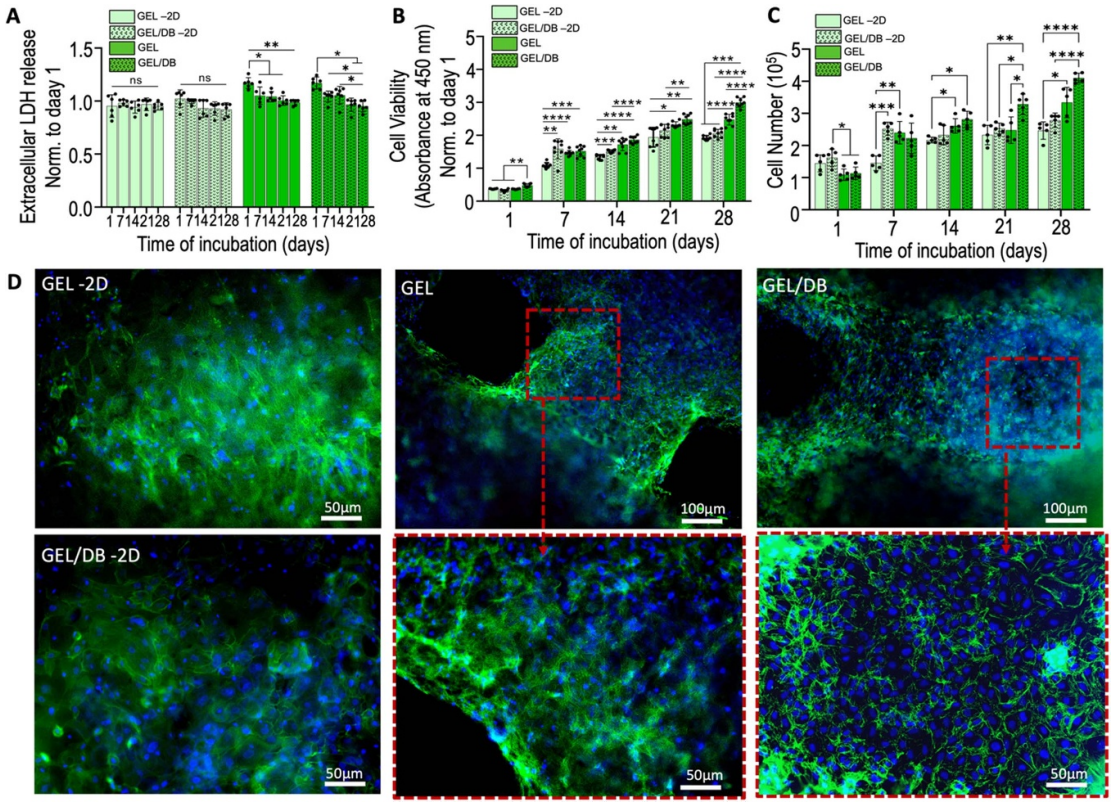

Figure 5. Cell growth inside GEL and GEL/DB constructs. (A) Extracellular LDH release of cells with statistical differences. (B) WST-8 viability assay quantified according to metabolic activity of cells. ($n = 6$, mean ± SD) (C) total cell number in cell-laden constructs ($n = 6$) calculated by PicoGreen dsDNA assay. Data are represented by mean ± SD in comparison between groups. $^{*}p < 0.05$, $^{**}p < 0.01$, $^{***}p < 0.001$, $^{****}p < 0.0001$ indicate statistically significant differences. (D) Confocal microscopy images of MC3T3-E1 pre-osteoblasts inside 2D cast (scale bars 50 μm) and 3D-bioprinted constructs on day 28. Scale bars: 100 μm (first row) and 50 μm. (second row). DAPI: nuclei (blue), F-Actin 488: cytoskeleton (green). The image in the red dashes shows cell proliferation inside the constructs and the pore area. DB particles seen in blue/green color due to their autofluorescence.

culture period. In 2D cell culture, released extracellular LDH levels by cells were similar and no statistical differences were found during the 28 d incubation period (figure 5(A)). However, 3D bioprinted groups showed higher LDH levels notably on day 1 (figure 5(A)). This higher LDH level in the early days might be due to shear forces induced cell death during the 3D bioprinting process [38]. In the following culture days, extracellular LDH levels consistently decreased with statistical significance, indicating that the remaining cells survived and proliferated in the later culture period. MC3T3-E1 cell viability was quantified based on the metabolic activity of cells measured by WST-8 assay and the data shows that all groups exhibited gradual increase of viability throughout the culture period (figure 5(B)). In addition, higher cell viability was determined in 3D-bioprinted GEL and GEL/DB constructs and statistically significant differences were found compared to the 2D cast groups. Moreover, cells inside 3D bioprinted GEL/DB constructs showed the highest viability compared to the other groups (figure 5(B)).

3.3.2. Cell proliferation and morphology

The cell proliferation inside the bioprinted constructs was determined depending on the dsDNA quantification by PicoGreen assay. In accordance with the viability results based on metabolic activity (figure 5(B)), the cell number inside the bioprinted constructs gradually increased during the cell culture period (figure 5(C)). On the first day, the cell number inside the bioprinted constructs was lower than in the 2D cast hydrogels which might be the consequence of the higher LDH released on day one shown in figure 5(A). After day one, the cell number increased on day 7, then stayed stable during the culture period in the 2D cast hydrogel group. On the other hand, cells inside 3D-bioprinted constructs proceeded to proliferate for 28 d, and statistically significant differences were detected compared to the 2D hydrogels on days 7, 14 and 28. Furthermore, the highest cell number was quantified in bioprinted GEL/DB constructs with statistically significant differences compared to the 3D printed GEL group on day 21 (figure 5(C)). According to the cytotoxicity, viability and proliferation investigation, GEL and DB incorporated GEL bioinks provided a 3D microenvironment for cell growth after bioprinting and exhibited promising results as a natural-based minimalistic formulation of bioink.

Cell adhesion and cell morphology inside 3D bioprinted constructs and 2D cast hydrogels were

evaluated by fluorescence microscopy. DAPI and F-Actin stainings show the nucleus (blue), and cytoskeleton (green) of MC3T3-E1 cells, respectively. Microscopy images display cell adhesion in both 2D cast and 3D-bioprinted constructs as well as cell-material interaction after 28 d of culture period (figure 5(D)). 2D cast groups demonstrated the cell-material interaction on day 28 and cells covered the DB particles' surface inside the DB-incorporated GEL hydrogels (figure 5(D)). In the 3D-bioprinted GEL/DB group, cells covered the constructs exhibiting a very positive interaction with DB particles, in addition, cells covered the pore area on day 28, which can be seen in magnified images (figure 5(D)).

Fabricated MC3T3-E1 cell-laden GEL/DB constructs demonstrated positive cell-material interaction. Cell proliferation and growth inside the constructs were increased by the addition of DB particles into the GEL matrix. This improvement in cell behavior is assumed to be due to the collagen fibers and hydroxyapatite components present in the DB particles. It is estimated that natural bone histoarchitecture (that was preserved in the decellularization method) supported cell growth inside the GEL/DB constructs. Following the successful biofabrication of cell-laden GEL/DB constructs and obtaining promising cell response, we proceeded to bioprint hTERT-MSCs using DB particles of smaller size (45 μm) and higher concentration (10%). It was hypothesized that such inks could potentially lead to an even higher cell response.

3.4. Assessments of the different sizes and concentrations of DB particles on cell behavior of 3D-bioprinted hTERT-MSCs-laden GEL/DB constructs

The cell viability inside the 3D-bioprinted structures was evaluated by a Live/Dead staining. Fluorescence microscopy images revealed cell viability and growth inside the GEL and GEL/DB constructs during the 28 day culture period (figure 6). In addition, DB particles displayed a blue color due to the autofluorescence of the collagen fibers. On the first day, a high number of viable cells (green) were observed in all groups and cell clusters were detected, particularly in DB incorporated constructs. Due to the high particle density and their autofluorescence, hTERT-MSCs were not clearly visible on day one. Nevertheless, large green staining, especially in the 10% DB group, indicated the formation of cell clusters within the structures (figure 6). After 7 d, cells started to elongate and spread in the bioprinted constructs, afterwards cells maintained their viability and proliferated during the 28 d of culture period (SI figure 3(B)). The spreading of hTERT-MSCs was favorable, and complete cell coverage was observed on 28 d of culture. Moreover, the density of live cells was quite high on all incubation days. It was difficult to find dead cells (red) even on day 28, indicating that the ink formulations are cytocompatible and higher DB particle concentration supports cell growth.

The potential cytotoxicity of the ink material was quantified using a LDH cytotoxicity assay after bioprinting. Cell-laden constructs were cultured for 28 d, and extracellular LDH release was quantified from the cell culture supernatant at each time point. The results showed that the LDH level remained stable and did not increase in any group throughout the culture period. There were no statistical differences detected between time points and groups, which indicates that DB incorporated GEL composition had no cytotoxic effect on hTERT-MSCs (figure 7(A)). As shown also in the rabbit DB particles incorporated in GEL constructs (figures 4 and 5), bovine DB particles have no cytotoxicity effects on hTERT-MSC either.

Cell proliferation was evaluated using a PicoGreen assay based on the dsDNA quantification of the cell-laden constructs. The results showed that hTERT-MSCs proliferated with an increasing trend during 28 d of incubation (figure 7(B)). The cells inside the 10% DB-incorporated GEL constructs had the highest cell number at each time point in comparison to all groups. In addition, cell number significantly increased inside the DB incorporated constructs compared to the GEL constructs also, the cell number increased when the DB concentration increased as well. Increasing cell number may be associated with the addition of DB particles as well as the homogeneous distribution of the particles within the GEL matrix. The incorporation of DB particles significantly supported cell proliferation, which may be associated with the homogeneous distribution of the particles within the GEL matrix and the collagen and hydroxyapatite composition of DB particles (SI figure 2(C)). The incorporation of hydroxyapatite and the use of a variety of biopolymers in 3D-bioprinted structures were reported to considerably support cell proliferation and osteogenicity *in vivo* [39–41]. According to our cytotoxicity and proliferation assessment results, GEL/DB composite hTERT-MSCs-laden constructs had no cytotoxic effects and provide a proper environment for cell growth.

In order to evaluate the osteogenic differentiation capacity, 3D-bioprinted GEL/DB constructs were incubated for 28 d with (+OS) and without (−OS) an osteogenic induction medium. PicoGreen proliferation and ALP activity assays were used to assess hTERT-MSC differentiation to osteoblasts. According to the PicoGreen dsDNA determination results, hTERT-MSCs gradually proliferated inside 3D-bioprinted constructs in both the +OS and −OS groups (figure 7 (B) and (D)). The incorporation of the DB particles into the GEL matrix statistically increased cell proliferation. In addition, smaller sizes of DB particles significantly supported cell proliferation notably in the higher concentration (10% DB). Cell number was higher in the GEL/5 DB (45 μm)

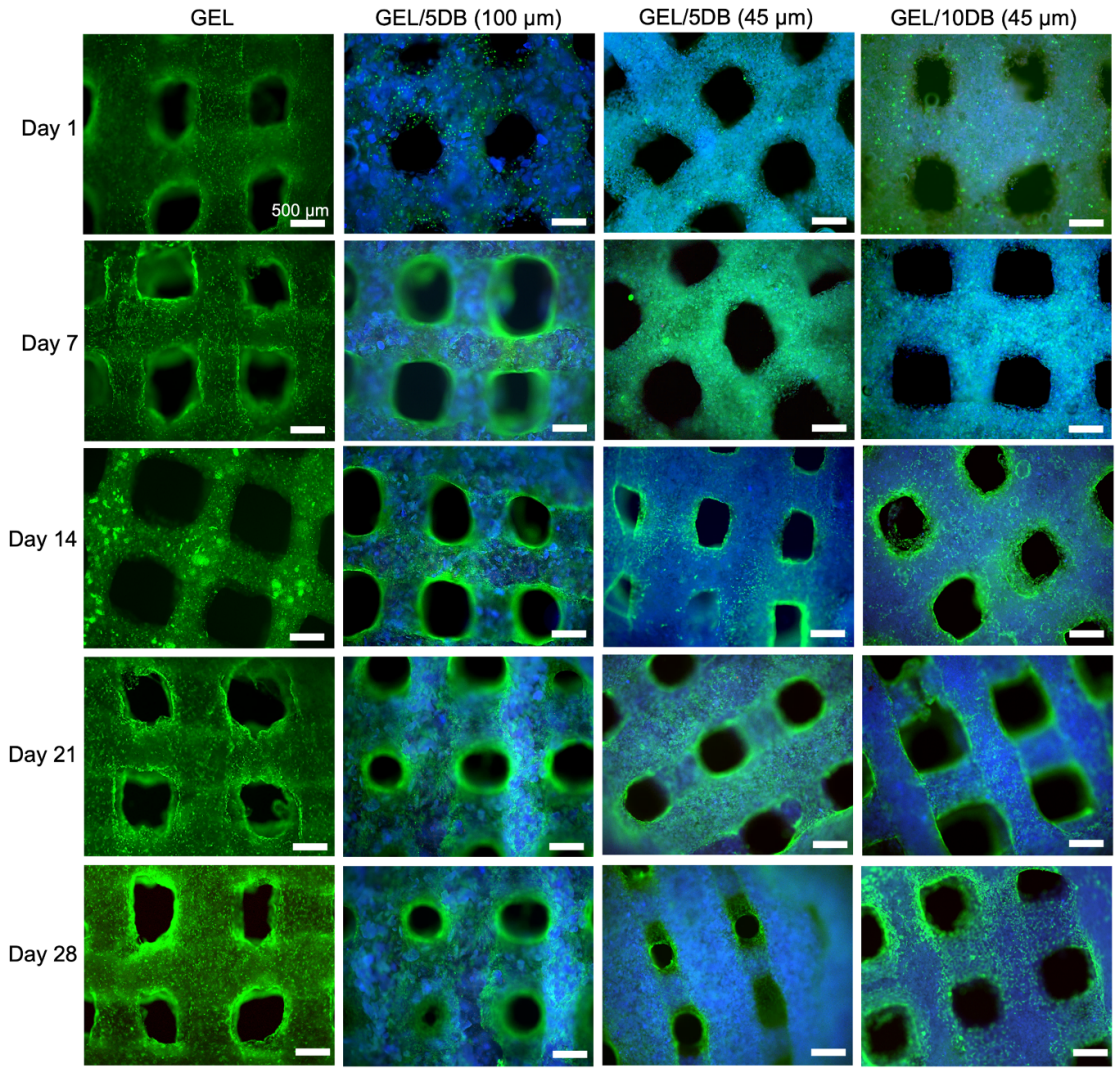

Figure 6. Live/Dead staining results of hTERT-MSC cells inside 3D-bioprinted GEL and GEL/DB composite constructs on days 14. Calcein AM (green) and EthBr (red) staining represent live and dead cells, respectively. DB particles are visible in blue color due to their autofluorescence property. Scale bars: 500 μm.

group compared to the GEL/5 DB (100 μm) group with significant differences at day 21 both in −OS and +OS conditions. The highest cell number was quantified on 28 d of the culture period in -OS induction groups (figure 7(B)). Also, MC3T3 pre-osteoblasts inside 1% DB incorporated GEL exhibited an increasing trend, however, a lower cell number was determined on day 28 when compared to the hTERT-MSCs. Although it was expected that the hTERT-MSCs would have a higher cell number due to their limitless proliferation capacity [42], it can be concluded that the increase in cell number may be caused by the DB particles. The collagen and hydroxyapatite content of DB particles (SI figure 2(C)) induced cell proliferation during the culture period; also, the GEL/10 DB group showed the highest cell number on day 28. A similar proliferation trend was observed in +OS induction groups although significant differences were predominantly detected between pure GEL and GEL/10 DB groups (figure 7(D)). On day seven, cells proliferate to a higher extent, compared to the −OS induction groups, afterward, the cells pursue proliferation, however, cell number did not increase significantly, which could be explained by cell differentiation, as shown in figure 7(E).

The ALP activity of hTERT-MSCs was assessed in both groups induced by +OS and −OS during the 28 d culture period. hTERT-MSCs are similar to primary MSCs, can be differentiated to osteoblasts and thus are routinely used in characterizing bone models [29]. As expected, ALP activity of hTERT-MSCs gradually increased in all groups induced by +OS during the culture period (figure 7(E)). In −OS groups, cells inside the pure GEL constructs showed a stable ALP activity. The highest activity was determined in the highest DB particles incorporated group in both +OS and −OS groups indicating that DB particles support the osteogenic activity. Interestingly, ALP activity of cells inside the DB incorporated constructs in −OS groups showed a statistically significant increase compared to the pure GEL group (figure 7(C)). This might be

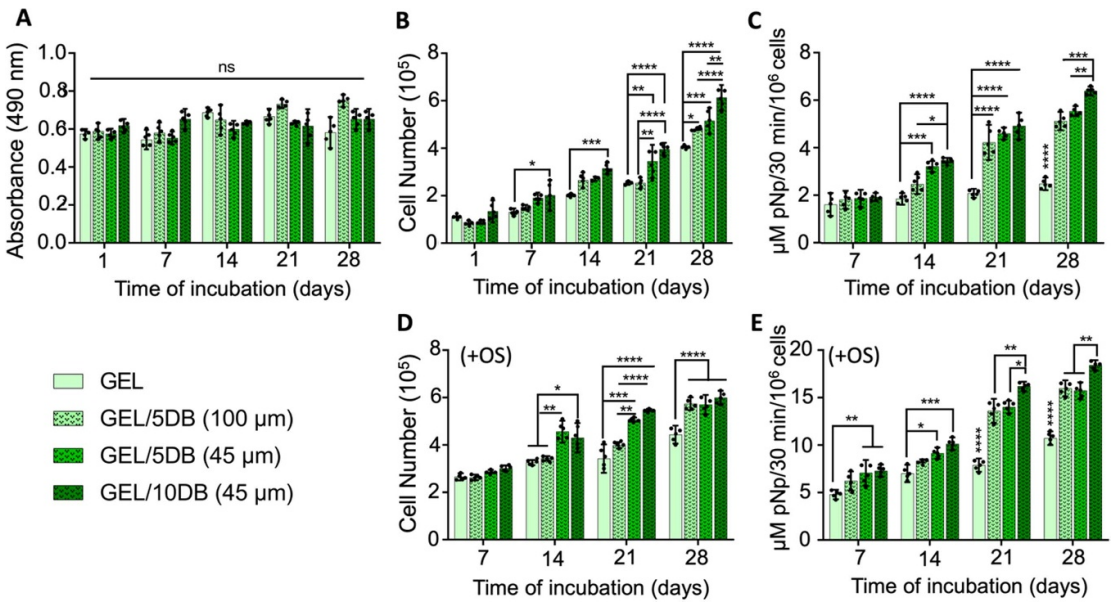

Figure 7. Biological activity of hTERT-MSC cells inside the bioprinted GEL/DB constructs. (A) Potential cytotoxicity determined by LDH assay. (B) PicoGreen dsDNA assay results show the total number of cells inside the bioprinted constructs. The differentiation capacity of cells was assessed by (D) total cell number and ALP secretion (C) without and (E) with osteogenic induction. ($n = 5$) Data are represented as mean ± SD. $^{*}p < 0.05$ and $^{**}p < 0.01$, $^{***}p < 0.001$ and $^{****}p < 0.0001$ indicate statistically significant differences of means between groups by one-way ANOVA tests.

caused by the hydroxyapatite composition of the DB particles as numerous studies reported hydroxyapatite particles induce osteogenicity [43, 44]. Many studies have demonstrated the supportive effect of inorganic materials, particularly hydroxyapatite, to support osteogenic differentiation capacity. Meesuk *et al* conducted an *in vitro* study using 3D-printed hydroxyapatite-based scaffolds seeded with MSCs, which showed significantly higher ALP activity and higher expression of osteogenic markers compared to the control group [45]. Moreover, ALP activity of +OS induced cells was higher almost three folds in each time point for all groups than for −OS groups. The natural biomineralization capacity of the DB particles and +OS induction significantly supported the osteogenic differentiation capacity of cells, a key hypothesis of our study. In accordance with our study, Gao *et al* demonstrated osteogenesis supported by pig DB particles in GelMA casted hydrogels, and also new tissue formation was observed *in vivo* [46]. Thus, it could be concluded that DB particles support osteogenesis and GEL/DB bioink formulation has the potential for bone tissue engineering applications.

The cell morphology and cell attachment inside the 3D-bioprinted constructs were evaluated in detail by confocal microscopy. DAPI and F-Actin stainings were used for cell nuclei (blue) and cytoskeleton (green), respectively (figure 8). In addition, DB particles inside the structures were visible (as a red/pink color) due to the autofluorescence of fibrous collagen in DB particles. The images indicate that cells grow and proliferate inside 3D-bioprinted constructs on day 28 (figure 8). Cells attached and elongated inside both GEL and GEL/DB constructs and a tendency of cell coverage was visible in all groups (SI. figures 4–7). Notably, a larger cell network and a good interaction with DB particles was observed in 10% DB incorporated GEL constructs. This cell adhesion demonstrated that cells interacted ideally with homogeneously distributed DB particles in the GEL/DB groups. In our previous study, we demonstrated that cells interacted with rabbit DB particles in freeze-dried GEL/DB scaffolds. The cells surrounded and attached to the rabbit DB particles and migrated toward the pores [21]. Here we also showed cell growth and attachment inside 3D-bioprinted constructs interacting with both rabbit (figure 5(D)) and bovine DB particles (figure 8). With the confirmation of the cell proliferation results, it can be concluded that the RGD sequence of the GEL matrix and the bone tissue-derived collagen fibers in DB particles induce cell attachment and proliferation. Confocal microscopy results revealed that both GEL and DB-incorporated GEL composite bioinks support cell–material interaction and allow cell growth inside the 3D bioprinted construct (SI figure 8). Furthermore, the biomaterials used in this study can all be found in clinical grade and in individual clinical use: both bioink compositions are composed of GEL already available as FDA approved composition [47], DB particles have already been proved for removal of the DNA content while maintaining collagen and GAGs composition [21]; mTG used as a crosslinker is also a FDA approved material [48]. Thus, our bioink formulation has potentially easier translatability than

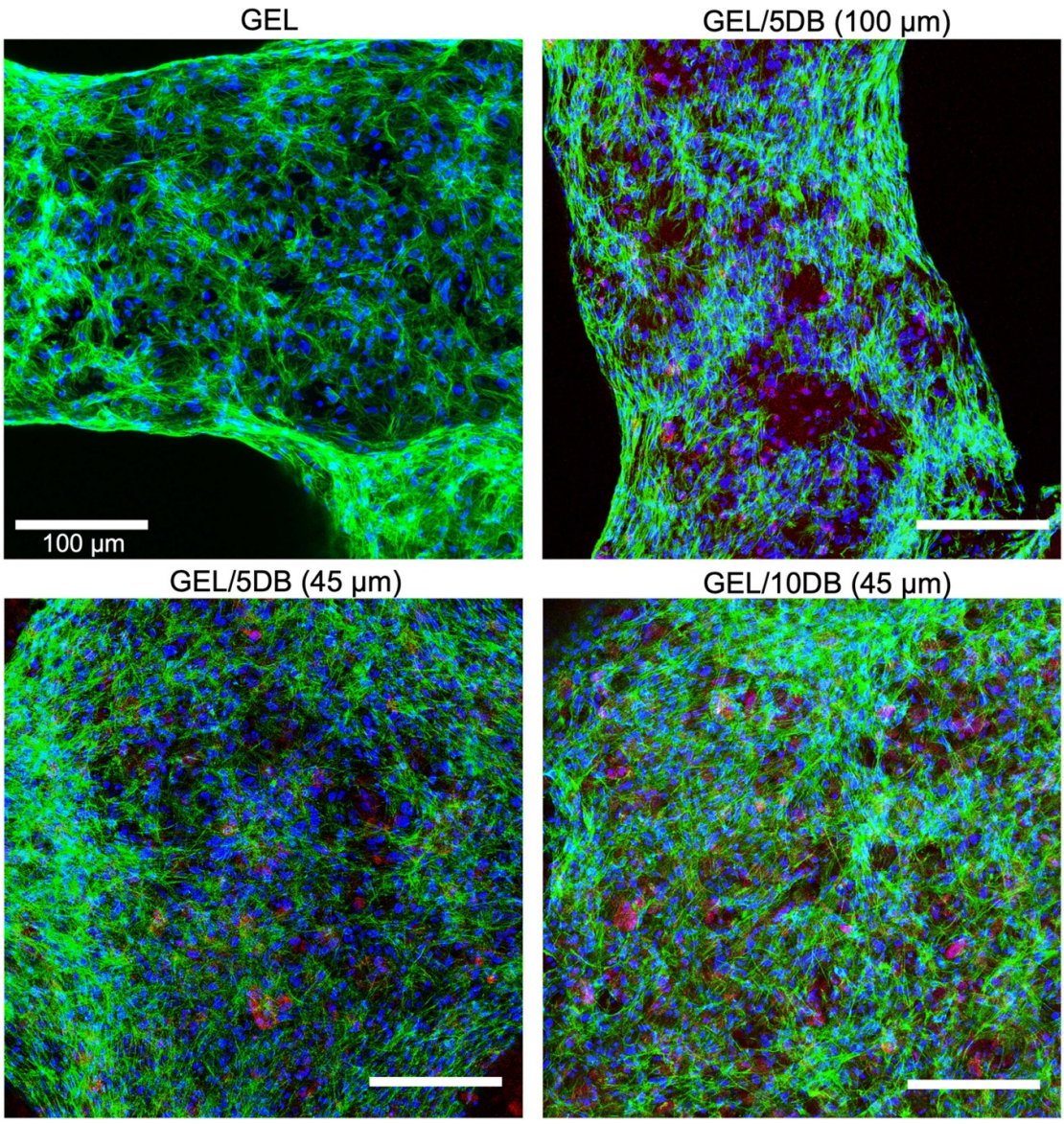

Figure 8. Confocal microscopy images of hTERT-MSCs growing inside the 3D bioprinted GEL and GEL/DB constructs at day 28 of culture. DAPI: nucleus (blue), F-Actin 488: cytoskeleton (green). DB particles are visible as red/pink areas due to their autofluorescence. Scale bars: 100 μm.

complex hydrogel systems which involve substantial modifications or components which are not available as clinical grade materials. In addition, when considering a patient with a fracture in clinical situation, the fractured bone (which is usually discarded in clinical surgery) can be prepared as particles and mixed with GEL, also including patient-derived cells. Then the bioink could be printed into defect-specific constructs for bone regeneration. This approach can also be used in reconstructive surgery.

4. Conclusions

In this study, we demonstrated a minimalistic bioink formulation composed of GEL, DB particles and MC3T3-E1 pre-osteoblasts or hTERT-MSCs, respectively. The main approach of our study is to utilize the natural ECM composition of bone tissue and to determine the ideal concentration of particles for better cellular response. The DB particles used in this study contain not only collagen fibers but also hydroxyapatite whereas existing studies used both decellularization and demineralization processes, which resulted in depletion of the biomineralization properties of bone. In addition, we present minimalist GEL-based bioink formulations with mTG crosslinking (an already FDA-approved material), which allows for straightforward preparation compared to complex hydrogel systems using many modifications or chemical components that may show cytotoxicity and are not available in clinical grade.

The incorporation of rabbit and bovine DB particles in different sizes and concentrations into the GEL matrix was assessed in terms of the biological activity of pre-osteoblasts and hTERT-MSCs. The viscosity, shape recovery and printability properties of the inks were evaluated and the effects of different DB particle concentrations and sizes were assessed. Moreover, the effect of the ink formulations on the biological activity of different cell types was investigated. The results provided a comparison of the different bioinks composed of 1%, 5%, 10% DB particles in terms of viscosity, printability and biological activity of the cells after 3D bioprinting. The DB incorporated-GEL combination was suitable for pre-osteoblasts and hTERT-MSCs bioprinting and provided an appropriate microenvironment for cell growth inside the bioprinted constructs. According to the printability assessment, the smaller size (45 μm) of DB particles allows for better 3D printing with higher particle (10%) concentration when compared with the 5% DB particles in 100 μm size. Reducing the DB particle size to 45 μm increased the viscosity and shape fidelity while enabling 3D printing with higher DB particle concentration. Notably, printability was enhanced when compared the 45 μm and 100 μm DB particles in 5% concentration. Regardless the origin of the bone particles (SI figure 1), DB incorporated GEL bioink formulations allow cell growth after 3D bioprinting for each concentration. The higher cell proliferation was determined in the GEL/10% DB particles (45 μm) group. Moreover, DB particles supported the osteogenic differentiation, notably ALP activity gradually increased in DB incorporated groups without osteogenic induction medium which might be due to the hydroxyapatite content of DB particles. Besides, the highest ALP activity was quantified in the GEL/10% DB group (45 μm). Therefore, we concluded that GEL/10% incorporating DB particles in 45 μm size is a suitable formulation for 3D bioprinting and supports hTERT-MSCs growth and osteogenic differentiation. 10% DB particles as a natural ECM source and the minimalistic GEL formulations offer promising bioinks for bioprinting applications for bone tissue engineering. Furthermore, since the smaller particle size provides better printability and allows using higher concentration of particles, different pulverization techniques could be considered to reduce particle size. Thus, a high amount of DB particles could interact with cells and might improve the cell growth and osteogenic differentiation capacity. Future work could include a comprehensive investigation focusing on *in vivo* studies and gene expression analysis to assess the functionality of GEL/DB bioinks. These are key factors determining the success of materials for bone tissue regeneration, and would allow predicting the suitability of different bioink formulations for clinical applications.

Data availability statement

All data that support the findings of this study are included within the article (and any supplementary files).

Acknowledgments

This study was supported by The Scientific and Technology Research Council of Turkey (TUBITAK 2214-A, International Doctoral Research Fellowship Program) and the Council of Higher Education of Turkey for 100/2000 PhD Scholarship in the field of Biomaterials and Tissue Engineering (CoHE 100/2000). The authors also would like to thank Professor Schieker's lab (Ludwig Maximilians University of Munich, Germany) for kindly providing hTERT MSCs.

Author contribution

AKÖ: conceptualization, methodology, investigation, material and experimental design, experiments, data analysis, writing of the original draft, review, and editing. TD: conceptualization, methodology, investigation, material and experimental design, review and editing. ARA: methodology, material and experimental design, confocal microscopy, review and editing. FT: conceptualization, methodology, review and editing, supervision. MG: conceptualization, methodology, resources, review and editing, supervision. ARB: conceptualization, methodology, resources, review and editing, supervision.

ORCID iDs

Aylin Kara Özenler https://orcid.org/0000-0001-8302-913X
Thomas Distler https://orcid.org/0000-0002-0319-3763
Ashwini Rahul Akkineni https://orcid.org/0000-0002-9611-8753
Funda Tihminlioglu https://orcid.org/0000-0002-3715-8253
Michael Gelinsky https://orcid.org/0000-0001-9075-5121
Aldo R Boccaccini https://orcid.org/0000-0002-7377-2955

References

[1] Groll J *et al* 2019 A definition of bioinks and their distinction from biomaterial inks *Biofabrication* **11** 13001
[2] Di Marzio N, Eglin D, Serra T and Moroni L 2020 Bio-fabrication: convergence of 3D bioprinting and nano-biomaterials in tissue engineering and regenerative medicine *Front. Bioeng. Biotechnol.* **8** 521853
[3] Marques C F, Diogo G S, Pina S, Oliveira J M, Silva T H and Reis R L 2019 Collagen-based bioinks for hard tissue

engineering applications: a comprehensive review *J. Mater. Sci., Mater. Med.* **30** 32
[4] Zhu H, Monavari M, Zheng K, Distler T, Ouyang L, Heid S, Jin Z, He J, Li D and Boccaccini A R 2022 3D bioprinting of multifunctional dynamic nanocomposite bioinks incorporating cu-doped mesoporous bioactive glass nanoparticles for bone tissue engineering *Small* **18** 2194996
[5] Irmak G, Demirtaş T T and Gümüşderelioğlu M 2019 Highly methacrylated gelatin bioink for bone tissue engineering *ACS Biomater. Sci. Eng.* **5** 831–45
[6] Ghorbani F *et al* 2023 Photo-cross-linkable hyaluronic acid bioinks for bone and cartilage tissue engineering applications *Int. Mater. Rev.* **68** 1–42
[7] Soliman B G *et al* 2023 Programming delayed dissolution into sacrificial bioinks for dynamic temporal control of architecture within 3D-bioprinted constructs *Adv. Funct. Mater.* **33** 2210521
[8] Liu W *et al* 2017 Extrusion bioprinting of shear-thinning gelatin methacryloyl bioinks *Adv. Healthcare Mater.* **6** 1601451
[9] Asim S, Tabish T A, Liaqat U, Ozbolat I T and Rizwan M 2023 Advances in gelatin bioinks to optimize bioprinted cell functions *Adv. Healthcare Mater.* **12** 2203148
[10] Guo L, Colby R H, Lusignan C P and Whitesides T H 2003 Kinetics of triple helix formation in semidilute gelatin solutions *Macromolecules* **36** 9999–10008
[11] Yue K, Trujillo-de Santiago G, Alvarez M M, Tamayol A, Annabi N and Khademhosseini A 2015 Synthesis, properties, and biomedical applications of gelatin methacryloyl(GelMA) hydrogels *Biomaterials* **73** 254–71
[12] Khayat A, Monteiro N, Smith E E, Pagni S, Zhang W, Khademhosseini A and Yelick P C 2017 GelMA-encapsulated hDPSCs and HUVECs for dental pulp regeneration *J. Dent. Res.* **96** 192–9
[13] Heid S, Becker K, Byun J, Biermann I, Neščáková Z, Zhu H, Groll J and Boccaccini A R 2022 Bioprinting with bioactive alginate dialdehyde-gelatin (ADA-GEL) composite bioinks: time-dependent in-situ crosslinking via addition of calcium-silicate particles tunes in vitro stability of 3D bioprinted constructs *Bioprinting* **26** e00200
[14] Zou S, Fan S, Oliveira A L, Yao X, Zhang Y and Shao H 2022 3D printed gelatin scaffold with improved shape fidelity and cytocompatibility by using antheraea pernyi silk fibroin nanofibers *Adv. Fiber Mater.* **4** 758–73
[15] Giorleo L, Tegazzini F and Sartore L 2021 3D printing of gelatin/chitosan biodegradable hybrid hydrogel: critical issues due to the crosslinking reaction, degradation phenomena and process parameters *Bioprinting* **24** e00170
[16] de Barros N R *et al* 2023 Gelatin methacryloyl and laponite bioink for 3D bioprinted organotypic tumor modeling *Biofabrication* **15** 45005
[17] Negrini N C, Celikkin N, Tarsini P, Farè S and Święszkowski W 2020 Three-dimensional printing of chemically crosslinked gelatin hydrogels for adipose tissue engineering *Biofabrication* **12** 025001
[18] Yokoyama K, Nio N and Kikuchi Y 2004 Properties and applications of microbial transglutaminase *Appl. Microbiol. Biotechnol.* **64** 447–54
[19] Zhou M, Lee B H, Tan Y J and Tan L P 2019 Microbial transglutaminase induced controlled crosslinking of gelatin methacryloyl to tailor rheological properties for 3D printing *Biofabrication* **11** 25011
[20] Kreller T, Distler T, Heid S, Gerth S, Detsch R and Boccaccini A R 2021 Physico-chemical modification of gelatine for the improvement of 3D printability of oxidized alginate-gelatine hydrogels towards cartilage tissue engineering *Mater. Des.* **208** 109877
[21] Kara A, Distler T, Polley C, Schneidereit D, Seitz H, Friedrich O, Tihminlioglu F and Boccaccini A R 2022 3D printed gelatin/decellularized bone composite scaffolds for bone tissue engineering: fabrication, characterization and cytocompatibility study *Mater. Today Bio* **15** 100309
[22] Bednarzig V, Schrüfer S, Schneider T C, Schubert D W, Detsch R and Boccaccini A R 2022 Improved 3D printing and cell biology characterization of inorganic-filler containing alginate-based composites for bone regeneration: particle shape and effective surface area are the dominant factors for printing performance *Int. J. Mol. Sci.* **23** 4750
[23] Richter R F, Ahlfeld T, Gelinsky M and Lode A 2019 Development and characterization of composites consisting of calcium phosphate cements and mesoporous bioactive glass for extrusion-based fabrication *Materials* **12** 122022
[24] Guduric V, Belton N, Richter R F, Bernhardt A, Spangenberg J, Wu C, Lode A and Gelinsky M 2021 Tailorable zinc-substituted mesoporous bioactive glass/alginate-methylcellulose composite bioinks *Materials* **14** 51225
[25] Monavari M, Homaeigohar S, Fuentes-Chandía M, Nawaz Q, Monavari M, Venkatraman A and Boccaccini A R 2021 3D printing of alginate dialdehyde-gelatin (ADA-GEL) hydrogels incorporating phytotherapeutic icariin loaded mesoporous SiO2-CaO nanoparticles for bone tissue engineering *Mater. Sci. Eng.* C **131** 112470
[26] Liu S, Kilian D, Ahlfeld T, Hu Q and Gelinsky M 2023 Egg white improves the biological properties of an alginate-methylcellulose bioink for 3D bioprinting of volumetric bone constructs *Biofabrication* **15** 025013
[27] Richter R F, Ahlfeld T, Gelinsky M and Lode A 2023 Composites consisting of calcium phosphate cements and mesoporous bioactive glasses as a 3D plottable drug delivery system *Acta Biomater.* **156** 146–57
[28] Özenler A K, Distler T, Tihminlioglu F and Boccaccini A R 2023 Fish scale containing alginate dialdehyde-gelatin bioink for bone tissue engineering *Biofabrication* **15** 025012
[29] Böcker W *et al* 2008 Introducing a single-cell-derived human mesenchymal stem cell line expressing hTERT after lentiviral gene transfer *J. Cell. Mol. Med.* **12** 1347–59
[30] Ouyang L, Yao R, Zhao Y and Sun W 2016 Effect of bioink properties on printability and cell viability for 3D bioplotting of embryonic stem cells *Biofabrication* **8** 035020
[31] Soltan N, Ning L, Mohabatpour F, Papagerakis P and Chen X 2019 Printability and cell viability in bioprinting alginate dialdehyde-gelatin scaffolds *ACS Biomater. Sci. Eng.* **5** 2976–87
[32] Lode A, Meissner K, Luo Y, Sonntag F, Glorius S, Nies B, Vater C, Despang F, Hanke T and Gelinsky M 2014 Fabrication of porous scaffolds by three-dimensional plotting of a pasty calcium phosphate bone cement under mild conditions *J. Tissue Eng. Regen. Med.* **8** 682–93
[33] Schwab A, Levato R, D'Este M, Piluso S, Eglin D and Malda J 2020 Printability and shape fidelity of bioinks in 3D bioprinting *Chem. Rev.* **120** 11028–55
[34] Wilson S A, Cross L M, Peak C W and Gaharwar A K 2017 Shear-thinning and thermo-reversible nanoengineered inks for 3D bioprinting *ACS Appl. Mater. Interfaces* **9** 43449–58
[35] Lee M, Bae K, Levinson C and Zenobi-Wong M 2020 Nanocomposite bioink exploits dynamic covalent bonds between nanoparticles and polysaccharides for precision bioprinting *Biofabrication* **12** 25025
[36] Lee M, Bae K, Guillon P, Chang J, Arlov Ø and Zenobi-Wong M 2018 Exploitation of cationic silica nanoparticles for bioprinting of large-scale constructs with high printing fidelity *ACS Appl. Mater. Interfaces* **10** 37820–8
[37] Klotz B J, Gawlitta D, Rosenberg A J W P, Malda J and Melchels F P W 2016 Gelatin-methacryloyl hydrogels: towards biofabrication-based tissue repair *Trends Biotechnol.* **34** 394–407
[38] Fischer L *et al* 2022 Calcium supplementation of bioinks reduces shear stress-induced cell damage during bioprinting *Biofabrication* **14** 45005
[39] Wenz A, Borchers K, Tovar G E M and Kluger P J 2017 Bone matrix production in hydroxyapatite-modified hydrogels suitable for bone bioprinting *Biofabrication* **9** 44103

[40] Soleymani S and Naghib S M 2023 3D and 4D printing hydroxyapatite-based scaffolds for bone tissue engineering and regeneration *Heliyon* **9** e19363
[41] Wang X-F, P-j L, Song Y, Sun Y-C, Wang Y-G and Wang Y 2016 Nano hydroxyapatite particles promote osteogenesis in a three-dimensional bio-printing construct consisting of alginate/gelatin/hASCs *RSC Adv.* **6** 6832–42
[42] Wang Y, Pei Y A, Sun Y, Zhou S, Zhang X-B and Pei M 2021 Stem cells immortalized by hTERT perform differently from those immortalized by SV40LT in proliferation, differentiation, and reconstruction of matrix microenvironment *Acta Biomater.* **136** 184–98
[43] Juhl O J, Merife A-B, Zhang Y, Lemmon C A and Donahue H J 2021 Hydroxyapatite particle density regulates osteoblastic differentiation through β-catenin translocation *Front. Bioeng. Biotechnol.* **8** 591084
[44] Zhou H and Lee J 2011 Nanoscale hydroxyapatite particles for bone tissue engineering *Acta Biomater.* **7** 2769–81
[45] Meesuk L, Suwanprateeb J, Thammarakcharoen F, Tantrawatpan C, Kheolamai P, Palang I, Tantikanlayaporn D and Manochantr S 2022 Osteogenic differentiation and proliferation potentials of human bone marrow and umbilical cord-derived mesenchymal stem cells on the 3D-printed hydroxyapatite scaffolds *Sci. Rep.* **12** 19509
[46] Gao C, Saw W and Wang Y 2021 Hydrogel composite scaffolds with an attenuated immunogenicity component for bone tissue engineering applications *J. Mater. Chem.* B **9** 2033–41
[47] Elzoghby A O 2013 Gelatin-based nanoparticles as drug and gene delivery systems: reviewing three decades of research *J. Control. Release* **172** 1075–91
[48] Duarte L, Matte C R, Bizarro C V and Ayub M A Z 2019 Review transglutaminases: part II-industrial applications in food, biotechnology, textiles and leather products *World J. Microbiol. Biotechnol.* **36** 11